Corrosion behavior of Additively Manufactured Ti-6Al-4V parts and the effect of post annealing

Ali Hemmasian Ettefagh
Ph.D. Candidate

Faculty Advisor: Professor Shengmin Guo

ABSTRACT

This paper evaluates the corrosion behavior of Ti-6Al-4V alloy parts produced by the method of laser-based powder bed fusion additive manufacturing (AM). The effect of post annealing heat treatment on the corrosion resistance is also studied by comparing the heat treated samples with cold rolled commercial titanium alloy samples. The results obtained via corrosion tests show that the corrosion rate of as-fabricated AM parts is almost sixteen times worse than the commercial grade samples. The accelerated rate was due to the presence of non-equilibrium phases and can be ameliorated by a proper post heat treatment process at 800°C for 2 hours. The proposed heat treatment makes the corrosion behavior of AM parts comparable to the commercial grade samples, dominated by the stress relief of the martensitic phase and formation of BCC phase of β Ti-6Al-4V which has a higher corrosion resistance. CALculation of PHAse Diagrams (CALPHAD) methods were used to identify the equilibrium phases.

In this study, the AM samples were prepared using a Concept-Laser GmbH Mlab-cusing-R system. Titanium alloy Ti-6Al-4V powders were supplied by Concept-Laser. Wrought (cold rolled) Ti-6Al-4V specimens with the same chemical compositions were acquired from a commercial supplier to compare their behavior with the AM samples. A standard corrosion cell with 3 electrodes was used to conduct corrosion tests, including a reference saturated calomel electrode (SCE), a counter electrode (platinum), and the samples to be studied as the working electrode. During corrosion tests, this fixed size open area was exposed to a 3.5 wt% NaCl water solution. A CHI-604C corrosion test instrument was used to obtain the open circuit potential (OCP) curves over a long duration (~30 hours) and to obtain Tafel curves within the potential range -1 VSCE to +1.5 VSCE with a scan rate of 1.67 mV/s. Prior to the corrosion tests, the sample surfaces were prepared by polishing with sand paper (grit size 320-1000), rinsing, and soaking in the test environment for both the OCP and polarization tests. For EIS measurements, the frequency range was 0.01 Hz to 100 kHz at $E=E_{(Open\ Circuit)}$. After gathering EIS curves, the experimental data were analyzed with the electrochemical software of the CHI-604C to generate the equivalent circuits.

According to Figure 18, the open circuit potential of the samples move, with increasing time, toward more positive values (anodic direction) which indicates the formation of a passive film on the surface of all samples. Furthermore, the surface potentials become stabilized after about 20 h for wrought, as-fabricated AM and heat treated AM samples and the final stabilized potential for the as-fabricated AM sample is slightly higher than the others. Besides, it is clear that the general corrosion behavior of the as-printed sample has deteriorated compared to the wrought samples, based on the shift of the related curve to a higher current density. After the heat treatment process, it can be seen that HT600 and HT800 curves have shifted towards lower current densities and this shift is more noticeable for the HT800 case, indicating the lowest corrosion rate among the AM samples.

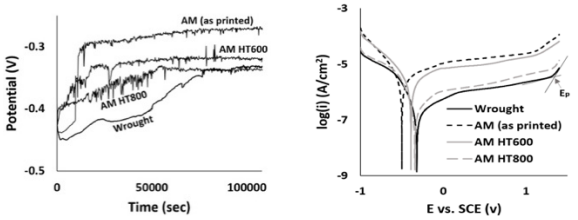

Figure 18- (left) Open circuit potential as a function of time, and (right) Tafel curves of the tested samples.

In order to further confirm the above findings, EIS measurements were performed to evaluate the corrosion mechanism by obtaining the Bode and Nyquist plots and their associated equivalent circuits. Figure 19-d that the wrought sample having the highest arc radius followed by the AM HT800 sample. In addition, according to the Bode plots (Figure 19-b,c), at high frequencies, the log |Z| metric trends towards constant values while the phase angle values drop to zero at high frequencies. In the range of medium to low frequencies, the phase angle values approach 90 degrees suggesting that a protective film (i.e. passive layer) has been formed on all of the samples in the solution. A result which is supported by the attained Tafel curves. Furthermore, the higher values of phase angle in the wrought sample indicate a more protective passive film compared to the as-printed sample.

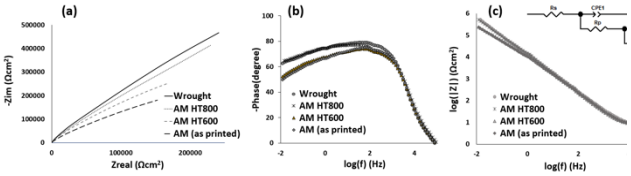

Figure 19- (a) Nyquist plots and (b),(c) Bode plots of all samples accompanied with (d) the electric equivalent circuit. All tests were performed in 3.5wt% NaCl water solution.

XRD profiles of all samples can be seen in Figure 20. It is clear that the same phases are present at the same angles of diffraction (2θ), but with different intensities, for the tested samples. Both wrought and AM samples consist of mainly hexagonal Ti (α) with the preferred crystal direction of (101) and a BCC phase (β) which is more obvious in the wrought sample. It is noticeable that α peaks in the AM samples are broader relative to the same peaks of wrought samples suggesting a non-equilibrium phase structure (α′). The existence of a non-equilibrium phase structure is due to the rapid solidification during the LPBF process. This thermal regime prevents the diffusion of vanadium and as a result, α′ has a higher content of vanadium compared to α phase.

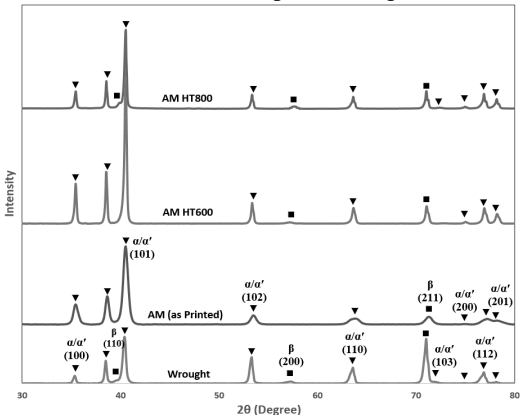

Figure 20- X-ray diffraction pattern of the AM and wrought samples of Titanium alloy Ti-6Al-4V. Both as-printed AM samples and samples undergone heat treatment are shown. ■ bullets represent β phase and ▼ bullets indicate the α or α′ phase.

Figure 21 presents the SEM images showing the microstructure of the samples. As can be seen, the wrought sample primarily consists of equilibrium α and β phases (dark and light areas respectively).

In order to provide a more systematic evaluation of equilibrium phases of this alloy, the CALPHAD method was applied. For this purpose ThermoCalc software and the TCTI1 thermodynamic database were used to obtain the phase diagram of the alloy at different temperatures under equilibrium conditions along with the chemical compositions of each phase at 500°C. These results are presented in Figure 22 and are in agreement with with pervious results.

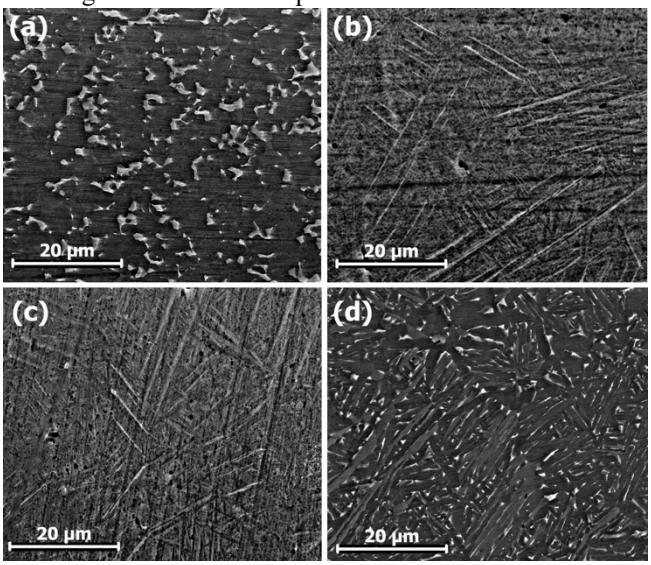

Figure 21- Microstructure of Ti6Al4V: wrought or AM and heat treated at different temperatures for 2 hr , a) Wrought, (b) AM (as-printed), (c) AM HT600, and d) AM HT800. Lighter zones in wrought and HT800 samples are β phase, and the dark phase is α phase.

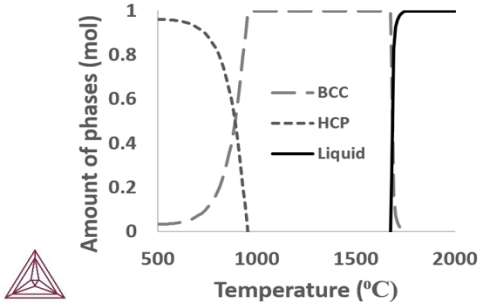

Figure 22- Stable phases at different temperatures under equilibrium solidification condition based on CALPHAD calculations by Thermocalc software.

ACKNOWLEDGMENTS

The current work is supported by the NSF EPSCoR CIMM project under award #OIA-1541079.

REFERENCES

[1] ActaMaterialia, vol. 61, no. 3, pp. 844-879, 2013.
[2] Corrosion Science, vol. 111, pp. 703-710, 2016.
[3] Materials & Design, vol. 63, pp. 185-193, 2014.
[4] Corrosion Science, vol. 43, no. 8, pp. 1465-1476, 2001.
[5] ElectrochimicaActa, vol. 56, no. 4, pp. 1746-1751, 2011.
[6] Computer-Aided Design, vol. 69, pp. 65-89, 2015.
[7] InTech, 2014, p. Chapter 1.
[8] Additive Manufacturing, vol. 22, pp. 153-156, 2018.